The innate origin of radial and vertical gradients in a simulated galaxy disc

Navarro, J.F.; Yozin, C.; Loewen, N.; Benítez-Llambay, A.; Fattahi, A.; Frenk, C.S.; ... ; Theuns, T.

MNRAS **000**, 1–13 (2016) Preprint 23 January 2019 Compiled using MNRAS LATEX style file v3.0

The innate origin of radial and vertical gradients in a simulated galaxy disc

Julio F. Navarro[1⋆], Cameron Yozin[1], Nic Loewen[1], Alejandro Benítez-Llambay[2], Azadeh Fattahi[1], Carlos S. Frenk[2], Kyle A. Oman[1], Joop Schaye[3], Tom Theuns[2].
[1] *Department of Physics and Astronomy, University of Victoria, Victoria, BC, Canada V8P 5C2*
[2] *Institute for Computational Cosmology, Department of Physics, Durham University, South Road, Durham, DH1 3LE, UK*
[3] *Leiden Observatory, Leiden University, PO Box 9513, 2300 RA Leiden, The Netherlands*

Accepted XXX. Received YYY; in original form ZZZ

ABSTRACT

We examine the origin of radial and vertical gradients in the age/metallicity of the stellar component of a galaxy disc formed in the APOSTLE cosmological hydrodynamical simulations. Many of these gradients resemble those in the Milky Way, and have been interpreted as due to internal evolutionary processes, such as scattering off giant molecular clouds, radial migration driven by spiral patterns, or orbital resonances with a central bar. In the simulation, however, these trends arise as a result of the gradual enrichment of a gaseous disc that is born thick but thins as it turns into stars and settles into centrifugal equilibrium. The vertical settling is controlled by the feedback of newly formed stars; as a result, the timescales of star formation, enrichment, and equilibration are linked, inducing clear radial and vertical gradients in the gaseous disc and its descendent stars. The kinematics of stars of given age evolve little after birth and thus provide a faithful snapshot of the gaseous disc structure at the time of their formation. In this interpretation, the age-velocity dispersion relation reflects the gradual thinning of the disc rather than the importance of secular orbit scattering; the outward flaring of stars results from the gas disc flare rather than from radial migration; and vertical gradients arise because the gas disc gradually thinned as it enriched. Our results, together with other recent cosmological simulations, support a scenario where disc stars reflect the properties of the gaseous discs at the time of their birth rather than the cumulative effect of secular evolutionary processes.

Key words: galaxies: kinematics and dynamics – galaxies: structure – galaxies: formation – galaxies: evolution

1 INTRODUCTION

The ages and metallicities of disc stars in the Milky Way (MW) show well-established radial, vertical, and kinematic gradients. In the solar neighbourhood, for example, the velocity dispersion of stars increases with age (e.g., Wielen 1977; Quillen & Garnett 2001; Holmberg et al. 2009), and age correlates in turn with total metallicity and, in particular, with the abundance of α elements at given [Fe/H] (e.g., Freeman & Bland-Hawthorn 2002; Haywood et al. 2013). In the disc midplane, the average age and metallicity of stars decline with increasing cylindrical radius, R (e.g., Boeche et al. 2013; Hayden et al. 2014). The radial age trend is preserved but the metallicity gradient appears to reverse when considering stars at fixed vertical distances, $|z|$, away from the disc symmetry plane (e.g., Anders et al. 2014; Bergemann et al. 2014; Martig et al. 2016; Ness et al. 2016).

At fixed R, the vertical scaleheight of stars increases with decreasing metallicity or increasing age (e.g., Mikolaitis et al. 2014; Casagrande et al. 2016); these gradients depend on R and become steeper at smaller radii (Hayden et al. 2014). Finally, at fixed metallicity, the vertical scaleheight of stars increases ('flares') from the centre outwards, especially for stars with low [α/Fe] ratios; the flare depends on metallicity, becoming more pronounced at lower [Fe/H] (Bovy et al. 2016).

Although the detailed form of each of these correlations vary somewhat from study to study, their qualitative nature seems robust. Their physical origin, however, is still a matter of debate. One possibility is that, to first order, the differences between old (metal-poor) stars and young (metal-rich) stars are driven by the integrated effect of secular evolution-

⋆ E-mail:jfn@uvic.ca

ary processes, such as orbital scattering off molecular clouds, radial migration induced by non-axisymmetric disc features, or dynamical heating by accretion events, external perturbations, and disc instabilities. These processes naturally affect older stars more, inducing vertical gradients and systematic trends between age/metallicity and kinematics that resemble the observed ones (for a review, see Rix & Bovy 2013, and references therein).

A contrasting view is that stellar gradients are largely imprinted at birth, and thus reflect the properties of the parent (gaseous) disc at the time of formation of each coeval stellar population. In this scenario, the star formation and enrichment history of the disc are linked to the evolution of its vertical structure and to the timescale of its dynamical equilibration (Brook et al. 2012; Bird et al. 2013; Stinson et al. 2013; Miranda et al. 2016; Ma et al. 2017; Grand et al. 2017). At early times the gaseous disc was thick and metal poor, but it enriched as it thinned down, leaving behind a strong vertical gradient in the age and metallicity of the stars at each fixed radius, in a process reminiscent of the classic Eggen et al. (1962) dissipative collapse picture. Radial gradients arise in this model simply because the gaseous disc assembles inside out and is denser near the centre, leading to faster transformation of gas into stars and more rapid enrichment than in the outskirts.

Each of these views has its pros and cons. For example, secular evolution models have difficulty accounting for the radially increasing scaleheight ('flare') of stars, since kinematic perturbations are expected to be weaker at larger radii on account of lower densities, and to proceed more slowly there because of longer orbital times. Birth models, on the other hand, have difficulty explaining why the vertical settling and enrichment timescales needed to explain the data are so much longer than the local dynamical timescale, which would naively be expected to set the collapse and equilibration timescale of the disc.

A further complication is the presence of an apparent 'gap' in the α vs Fe abundances of stars at fixed R, which has often been interpreted as signalling the presence of two disc populations of possibly distinct origin: a relatively old, α-rich 'thick' disc mixed with a younger, α-poor 'thin' population of overlapping [Fe/H] (see; e.g., Venn et al. 2004; Bensby et al. 2005; Navarro et al. 2011; Recio-Blanco et al. 2014, and references therein).

These complexities explain why 'chemodynamical' models have borrowed freely features from both formation scenarios to reproduce the structure of the Milky Way disc(s) (see; e.g., Matteucci & Francois 1989; Chiappini et al. 2001; Minchev et al. 2013, 2014, and references therein). Radial migration; external accretion; self-enrichment; gas outflows and inflows; these are some of the mechanisms invoked to reproduce the peculiar kinematic and chemical structure of the Galactic thin and thick discs. The models are complex, and the solutions often non-unique. In addition, the specificity of such models hinders their general applicability to understanding the relative importance of various physical mechanisms in a typical disc galaxy.

Direct cosmological hydrodynamical simulations of disc galaxy formation offer a complementary approach, where, modulo the algorithmic choices for simulating star formation and feedback, the roles of evolutionary effects and of conditions 'at birth' may be contrasted and assessed in statistically significant samples. The price to pay is that very few, if any, of the models will reproduce the detailed structure of the Milky Way, implying that the physical origin of observed Galactic trends must be inferred from judicious application of lessons learned from simulated galaxies that might not necessarily resemble our Galaxy in detail.

We adopt this approach here, where we analyze the formation of a disc galaxy in the APOSTLE[1] suite of cosmological hydrodynamical simulations of the Local Group (Sawala et al. 2016; Fattahi et al. 2016). Our analysis focusses on the physical origin of vertical and radial gradients of disc stars, on how they reflect the properties of the gaseous disc from which they descend, and on the effect of secular evolutionary processes that operate after their formation. Our paper is organized as follows. We describe briefly the APOSTLE numerical simulations in Sec. 2. Our main results are presented in Sec. 3. A toy model meant to illustrate how these results may be used to interpret the physical origin of vertical gradients is presented in Sec. 4. We end with a brief summary of our main conclusions in Sec. 5.

2 NUMERICAL SIMULATIONS

2.1 The APOSTLE project

The APOSTLE suite of zoomed-in ΛCDM cosmological hydrodynamical simulations evolves 12 volumes from a large cosmological box selected to resemble the main characteristics of the Local Group (LG). Each volume is centred on a pair of dark matter halos of combined virial[2] mass of order $\approx 2\times10^{12}\,M_\odot$. The pairs at lookback time $t=0$[3] are at a relative distance of $\approx 800\pm200$ kpc, approach with radial velocity of up to ≈ 250 km/s, have relative tangential velocities <100 km/s, and have no other halos of comparable mass within ≈ 2.5 Mpc. Details of the selection procedure are presented in Sawala et al. (2016); Fattahi et al. (2016).

All APOSTLE volumes were evolved with the same code developed for the EAGLE project (Schaye et al. 2015; Crain et al. 2015), which has been calibrated to reproduce some general properties of the galaxy population, such as the galaxy stellar mass function and the average size of galaxies as a function of mass. APOSTLE extends the EAGLE project to LG-like volumes and higher resolutions, using the fiducial choice of parameters (i.e., the 'Ref' model in the language of Schaye et al. 2015).

Each APOSTLE volume is resimulated at three different numerical resolutions, differing by successive factors of ≈ 10 in particle mass (labelled L1 to L3 in order of decreasing particle count). Our analysis will focus on one of the two main galaxies in volume AP-4-L2, using the nomenclature introduced by Fattahi et al. (2016). For that run, the high-resolution particle masses are $5.9\times10^5\,M_\odot$ (dark matter) and $1.2\times10^5\,M_\odot$ (gas). These particles interact with a

[1] A Project Of Simulating The Local Environment

[2] The virial properties of a dark matter halo are computed within spheres of mean density 200× the critical density for closure, $\rho_{\rm crit}=3H_0^2/8\pi G$. Virial quantities will be indicated with a '200' subscript.

[3] We shall hereafter use lookback time, t, to quote simulation results, in order to prevent confusion between 'redshift' and the vertical coordinate, z.

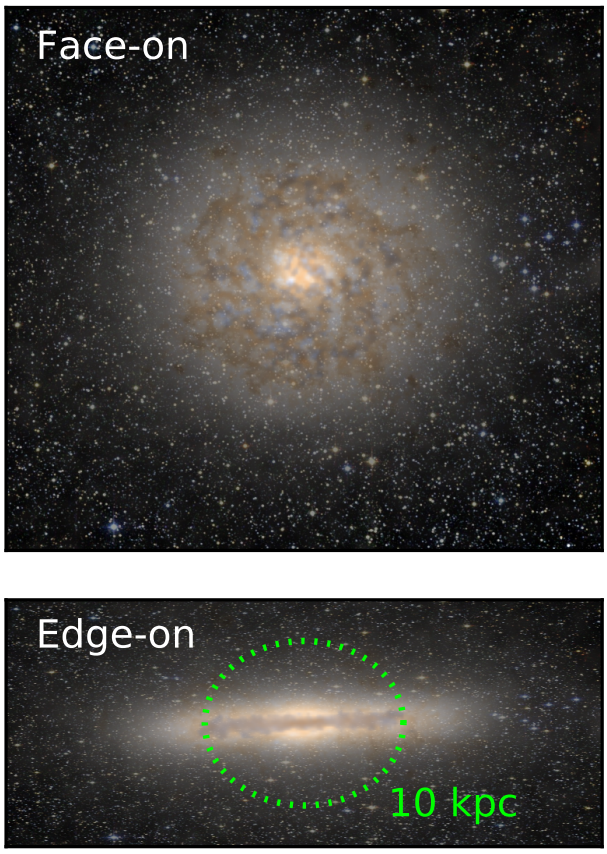

Figure 1. Mock image of the simulated galaxy at $t = 0$ seen face-on and edge-on. False colours use g, r, i broad bandpasses, as well as a simple prescription for dust absorption based on gas density and metallicity. The image is superposed on a artificial stellar field that mimics an image from the Hubble Space Telescope.

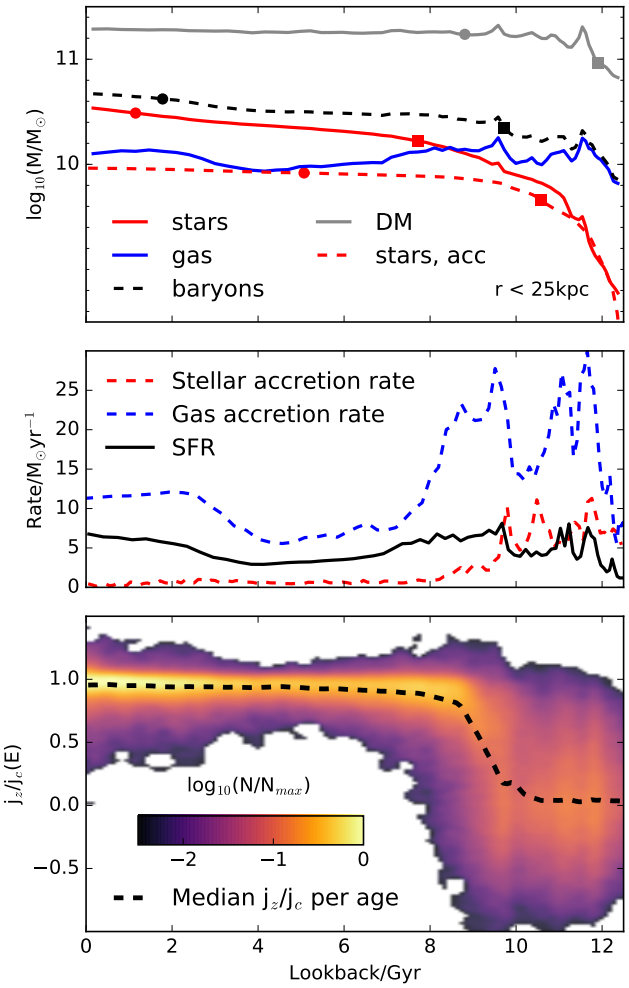

Figure 2. *Top panel:* Mass of various components of the galaxy within a fixed radius of 25 (physical) kpc from the galaxy centre, as a function of lookback time. Mass components include dark matter (grey solid line), baryons (black dashed), stars (red solid), accreted stars (red dashed), and gas (blue solid). The squares and circles in each curve indicate the time when, respectively, 50% and 90% of the final mass was in place. *Middle panel:* Gas (blue) and stellar (red) accretion rates, as a function of lookback time. The solid black line indicates the in-situ star formation rate. *Bottom panel:* Stellar age vs. circularity ($\epsilon_J = j_z/j_{\rm circ}(E)$) for all stellar particles in the galaxy at $t = 0$. Each pixel of the heat map is coloured according to a logarithmic function of particle number. Note that some particles have ϵ_J that slightly exceed unity; these are particles with $|z| > 0$ whose energies are compared with those of the midplane circular orbit at the same R. The black dashed line indicates the median circularity.

gravitational potential softened with a Plummer-equivalent spline kernel length fixed at 307 pc for $z < 3$ and constant in comoving units at higher redshifts.

APOSTLE runs assume a WMAP-7 cosmology throughout, with parameters $\Omega_{\rm M} = 0.2727$, $\Omega_\Lambda = 0.728$, $\Omega_{\rm b} = 0.04557$, $h = 0.702$ and $\sigma_8 = 0.807$ (Komatsu et al. 2011).

2.2 The simulated galaxy

Dark matter halos are identified using a friends-of-friends (FoF; Davis et al. 1985) algorithm run with linking length 0.2 times the mean interparticle separation. Individual self-bound structures within these halos are then identified recursively by the groupfinding algorithm SUBFIND (Springel et al. 2001; Dolag et al. 2009). The galaxies inhabiting the main subgroup of each FoF halo are referred to as 'centrals' and the rest as its 'satellites', if found within the virial radius of the central halo.

We focus our analysis on a single galaxy; the more massive of the pair of central galaxies in APOSTLE volume AP-4-L2. The properties of this galaxy are representative of other disc-dominated galaxies in APOSTLE; however, since our analysis involves the detailed tracking of individual star particles it is easier to illustrate our main results by focussing on a single galaxy. In particular, this galaxy was selected because, at $t = 0$, it (i) has a prominent disc of stars; (ii) shows no obvious morphological peculiarities; (iii) has formed stars steadily throughout its history; (iv) has had a relatively quiet recent merging history; and (v) has a gas/stellar mass ratio not unlike that of the Milky Way. We emphasize that this galaxy is *not* a model of the Milky Way. Fig. 1 shows face-on and edge-on views of the galaxy, in a box ≈ 50 kpc on a side.

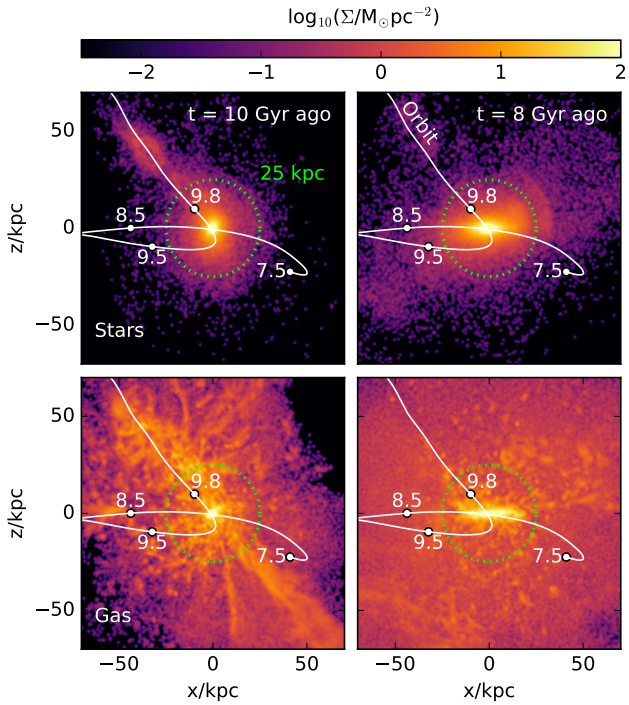

Figure 3. *Top row:* Projected distribution of stellar mass at two selected lookback times. The white solid line indicates the trajectory of the last major accreted satellite; labels indicate the location at given lookback time. *Bottom:* As top row, but for the gaseous component. The accreted satellite is part of a filamentary structure that accreted roughly at the same time, substantially increasing the gas mass of the galaxy. The satellite trajectory is as in the top row.

3 RESULTS

3.1 The assembly of the galaxy

The top panel of Fig. 2 shows the mass assembly history of the galaxy, as measured by the total mass of each component within a radius of 25 kpc (physical) from the centre of the progenitor halo. Most of the galaxy mass within that radius is assembled quickly: 50% of the dark matter mass was already in place 11.5 Gyr ago; the corresponding lookback time for the baryonic component is $t \approx 9.5$ Gyr.

Most baryons are accreted as gas and then turn gradually into stars, as shown in the middle panel of Fig. 2. Gas is delivered to the centre of the galaxy during an early period of rapid merging that is essentially over ≈ 9 Gyr ago. The last episode of early accretion is depicted in Fig. 3, where we see that the accretion of a substantial amount of gas along a filamentary structure accompanies a minor merger that happened roughly 10 Gyr ago.

After that accretion event the evolution of the galaxy is largely quiescent, except for an episode of gas accretion that started roughly 3 Gyr ago. This late accretion adds $\approx 10^{10}\,M_\odot$ of gas, but not many stars. This addition increases the final baryonic mass of the galaxy by $\approx 40\%$, but nearly doubles its gas mass at the time of accretion. The extra gas serves to ramp up the star formation rate of the galaxy at late times.

The middle panel of Fig. 2 also makes clear that the large majority of stars in this galaxy were born in situ[4]: fewer than $\approx 25\%$ of all stars at $t = 0$ formed in other systems, and roughly 90% of those were accreted more than ≈ 9 Gyr ago.

The quiet late merging history of the galaxy, together with the fact that most baryons are accreted in gaseous form, favour the formation of a centrifugally supported disc, as may be seen in the bottom panel of Fig. 2. This panel shows the circularity parameter of stars, $\epsilon_J = j_z/j_{\rm circ}$, measured at $t = 0$, as a function of their formation time. The parameter ϵ_J is defined as the z-component of the specific angular momentum of a star in units of that of a circular orbit of the same binding energy, and it therefore varies between ± 1 for stars in the midplane. Some stars may have ϵ_J slightly exceeding unity if they are outside the disc midplane. The z axis of the disc is defined at all times as the direction of the angular momentum vector of stars younger than 3 Gyr old.

Stars older than 10 Gyr formed before the early merging period of the galaxy was over: indeed, 80% of them are accreted and all together they have no net sense of rotation. Over the next ≈ 2 Gyr, however, a disc gradually forms and the average circularity climbs to unity. Stars formed during that epoch (i.e., ages between 8 and 10 Gyr) have a broad distribution of circularities, and the great majority (more than 70%) formed in-situ. Stars younger than ≈ 7 Gyr, on the other hand, nearly all formed in-situ and are found in approximately circular orbits in a thin coplanar disc (i.e., $\epsilon_J \approx 1$).

The various panels of Fig. 4 show a few snapshots[5] of the evolution of the galaxy. Here, from right to left, each column shows different orthogonal projections of stars formed, within a narrow interval of time, 10, 8, 4, and 0 Gyr ago, respectively. The first two rows show each coeval population of stars at $t = 0$. The third and fourth rows, on the other hand, show them at the time of their formation. The gas component of the galaxy is shown in the bottom two rows, for each time.

Fig. 4 shows that, as expected, stars trace, at the time of formation, the densest regions of the gaseous disc. Interestingly, however, the spatial configuration of stars evolves little after formation, and remains similar at $t = 0$. The stars of the simulated disc, therefore, seem to provide *today* a relatively faithful tracer of the properties of the gaseous disc at the time of their formation. This is the central result of our study, and will be a recurrent theme in the analysis that follows.

3.2 Age and metallicity gradients

The evolution of the gaseous disc discussed in the previous subsection leaves discernible gradients in the age and metallicity of its descendent stars at $t = 0$. We show this in Fig. 5, where the heat maps show, as a function of the

[4] At very early times, when only a small fraction of the final galaxy has been assembled, the main progenitor is not well defined. This leads to temporary uncertainties in the assignment of in-situ vs accreted stars. These uncertainties have no discernible consequences on our main conclusions.

[5] This figure was inspired by Fig. 1 of Ma et al. (2017).

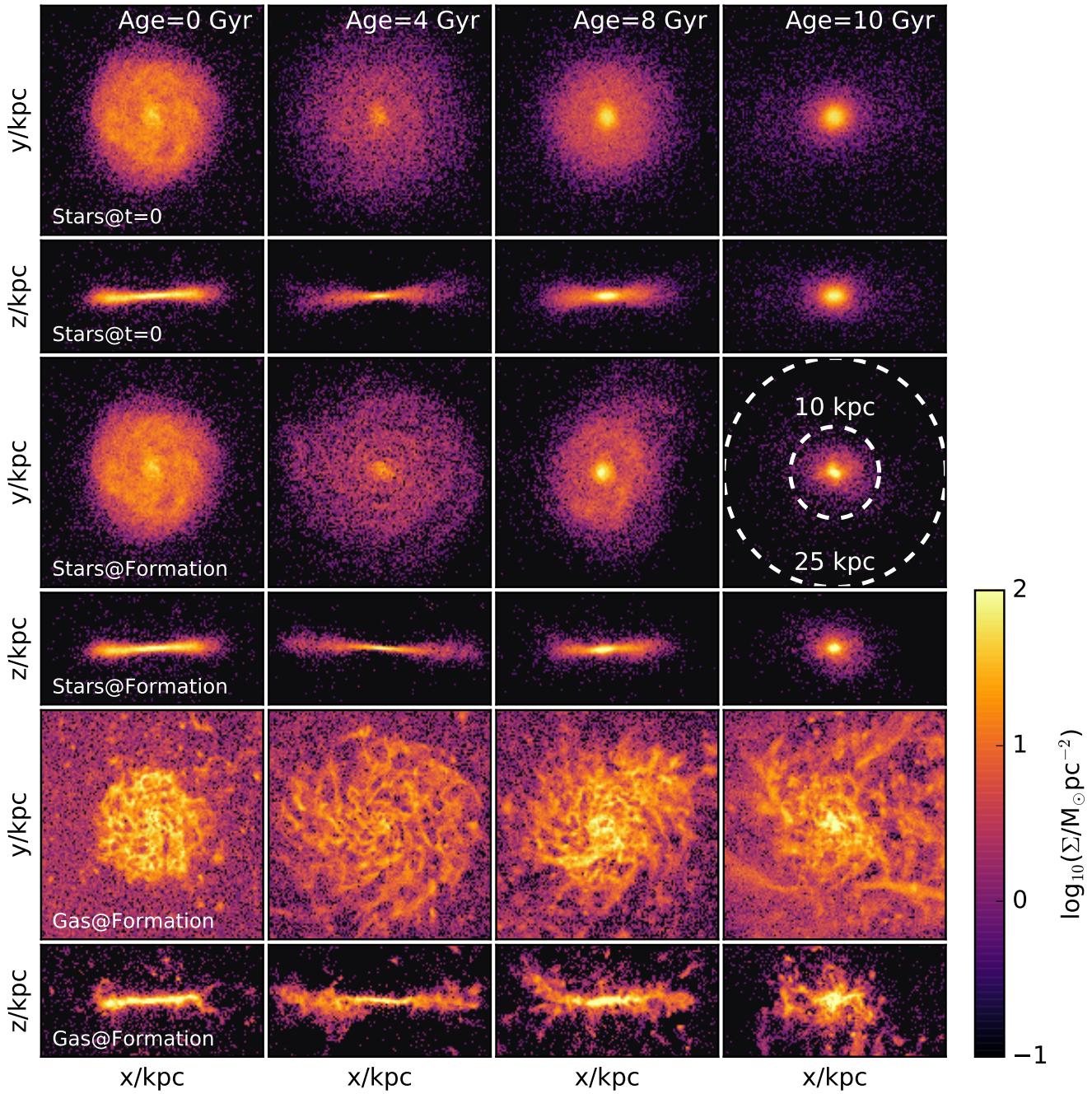

Figure 4. Face-on and edge-on projections of stars and gas at selected times. Top two rows show, at $t = 0$, stars with ages (± 0.5 Gyr) given in the legend of each box. Middle rows show the same stars as in the top rows, but as they were at the time of formation. Bottom rows indicate the gas component at each of the selected times. Note how the gas slowly assembles into a gradually thinning disc largely broken up into star forming clumps.

cylindrical coordinates, R and z, the average age and metallicity of stars. The gradients shown are characteristic of the 'inside-out/upside-down' disc formation scenario described in earlier work (see, e.g., Bournaud et al. 2009; Brook et al. 2012; Bird et al. 2013; Stinson et al. 2013; Miranda et al. 2016; Ma et al. 2017).

In the disc midplane the average age and metallicity decrease monotonically with increasing R. At fixed R, the ages of stars increase and their metallicities decrease with increasing $|z|$. These gradients are steeper near the centre of the galaxy than in its outskirts, implying that the characteristic scaleheight of stars of fixed metallicity (or age) 'flares' outwards. This flare is the reason why the radial metallicity gradient at fixed $|z|$ away from the plane 'inverts': for example, at fixed $|z| \approx 2$ kpc, the metallicity *increases* with R, a trend opposite to that seen in the midplane.

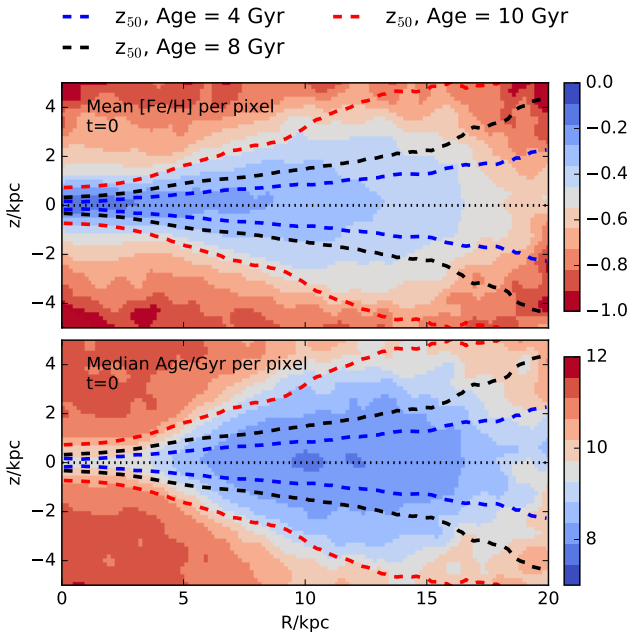

Figure 5. Average stellar metallicity (top) and age (bottom) of stars at the present time, as a function of the cylindrical coordinates R and z (colour labels on right). Note that the disc is strongly flared, and that younger stars delineate a thinner structure than their older counterparts. Dashed curves with different colours in both panels indicate the half-mass scaleheight of stars of ages 10, 8 and 4 Gyr. The origin of the strong radial and vertical gradients seen in this figure is the main focus of this paper.

3.3 The origin of radial and vertical gradients

The origin of the gradients highlighted in the previous subsection may be elucidated by contrasting the properties of stars at $t = 0$ with those of their parent gaseous disc at the time of their formation. We do this in Fig. 6, selecting for analysis stars formed between 4 and 10 Gyr ago. This period is simpler to analyze because it is characterized by a single major accretion episode, which, as discussed in Sec. 3.1, delivered a relatively large amount of gas to the forming galaxy. The accreted gas quickly assembles into a thick disc structure that slowly thins down as it forms stars (see; e.g., Fig. 4).

This evolution is depicted in the left column of Fig. 6, where, from top to bottom, we show the gas surface density profile, $\Sigma(R)$, its half-mass scaleheight profile, $z_{50}(R)$, and its average metallicity profile, [Fe/H](R), coloured as a function of time. These three panels show the evolution of a self-enriching, slowly thinning, flared gas disc that gradually transforms most of its gas into stars.

Interestingly, as shown in the right column of Fig. 6, stars show, at $t = 0$, a very similar structure to the gas in the radial and vertical directions, when selecting their ages to correspond to the same times chosen for the gas in the left panels. The clear correspondence between gas and stars as a function of time/age indicates that the origin of the stellar gradients lies in the evolving structure of the gaseous disc. Stars inherit the gas properties at birth and, to first order, preserve them until $t = 0$.

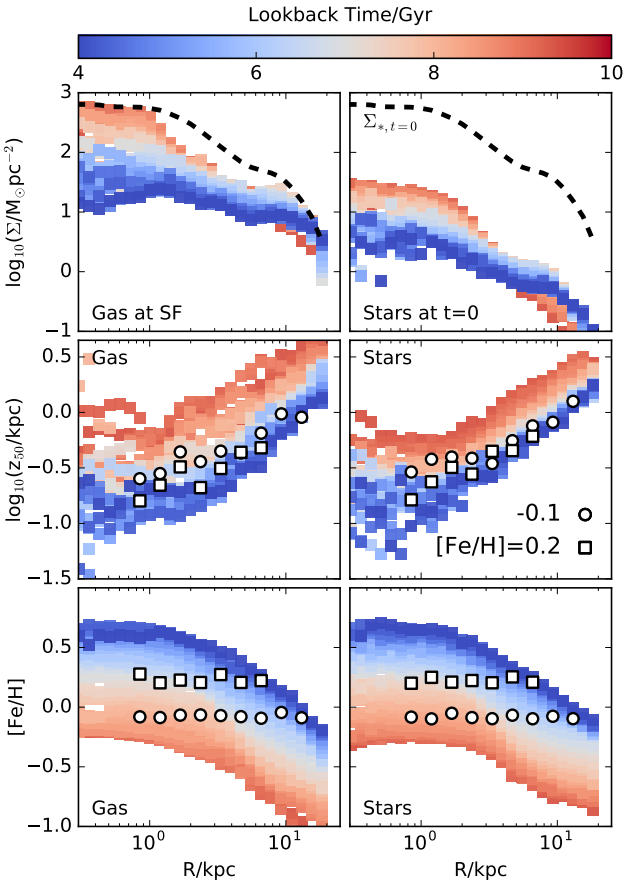

Figure 6. *Left column:* Surface density (top), half-mass scaleheight (middle) and average metallicity (bottom) radial profiles of the gas component of the simulated galaxy, at various times, as indicated by the colour bar at the top. Note that the gas gradually enriches itself as it settles vertically and makes stars. The thick dashed line in the top panel indicates the surface density profile of all stars at the present time, $t = 0$. *Right column:* Same as left, but for stars at $t = 0$, grouped by age. Note the tight correspondance between stellar gradients as a function of age and those of the gas at the time of their formation. Open circles and squares highlight populations of fixed metallicity, [Fe/H]$= -0.1$ and $+0.2$, respectively. (See Fig. 7 for further discussion.)

Note that because the gaseous disc is flared at all times, and thins down as it enriches, stars of fixed metallicity form at different times at different radii and with different scaleheights. The flare of stars of fixed metallicity thus reflects the flaring of the gas disc, modulated by the gradual thinning that occurs at each radius.

The open circles and squares in Fig. 6 illustrate this. These symbols track two different metallicities, [Fe/H]$=$ -0.1 and $+0.2$, respectively. In the bottom-left panel, the colour underneath each symbol indicates *at what lookback time*, as a function of radius, the average gas metallicity reached each of those values. In the bottom-right panel, on the other hand, the colours indicate, as a function of radius, *the ages* of stellar populations with each of those metallicities, at $t = 0$. The good agreement between gas and stars demonstrates that most stars have not migrated far from the radii where they were formed.

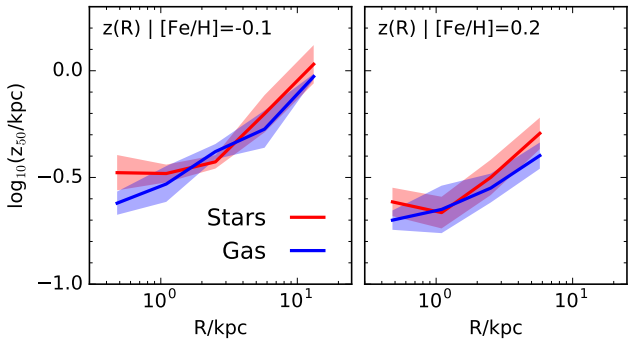

Figure 7. Red curves indicate the $t = 0$ half-mass scaleheight, z_{50}, as a function of radius R, for stars within 0.05 dex of [Fe/H]= −0.1 (left) and +0.2 (right). These correspond to the open circles and squares highlighted in the bottom panels of Fig. 6. Shaded bands indicate the rms scatter about the mean. The z_{50} radial dependence of each of those populations is in close agreement with the scaleheight of the gas at the time when, at each radius R, the average metallicity matched the selected value (see blue curves). This indicates that the 'flare' in stars of fixed metallicity is inherited from the properties of the gaseous disc at the time of their birth and evolves little thereafter.

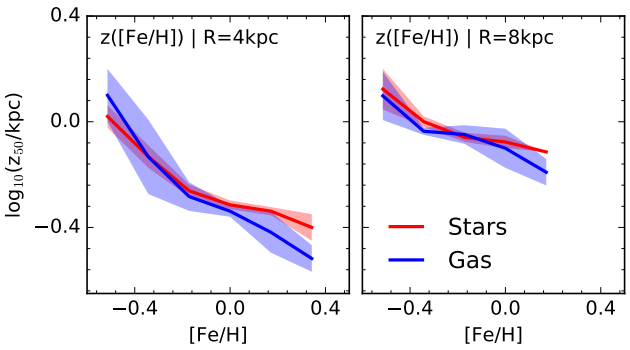

Figure 8. Half-mass scaleheight, z_{50}, as a function of metallicity, for stars found at the present time at two selected radii; $R = 4$ (red curve in left panel) and 8 kpc (red curve in right panel). As in Fig. 7, the blue curves in each panel indicate the evolution of the scaleheight of the gas, measured at the time when the average metallicity at each radius matched the value of [Fe/H] along the x-axis. The close agreement between gas and stars indicates that the vertical stellar gradient is due to the gradual enrichment of a slowly thinning gaseous disc. Stars inherit the properties of the gas at birth and largely preserve them to the present time.

The lookback times (for the gas) and ages (for the stars) mentioned in the preceding paragraph are then used in the middle panels of Fig. 6 to indicate the half-mass scaleheight of the gas at each of those times (left panel) or the half-mass scaleheight of the stars of each of those ages at $t = 0$. Again, the close resemblance between the flare of gas and stars selected in this way indicates that the stellar gradients originate in the properties of the gaseous disc at the time of the formation of each coeval stellar population.

One consequence of this resemblance is that, at $t = 0$, stars of fixed metallicity are flared (see Fig. 7). The steepness of the flare depends on a combination of several factors: how strong the gas disc flare is, how quickly the gas self-enriches, and how fast the disc thins down at various radii.

Had the disc thinned down much more rapidly, for example, so that at late times the scaleheight in the outskirts was similar to that of the inner regions at early times, the flare in stars of fixed metallicity would be much weaker, or might even disappear altogether. This interplay between thinning, enrichment, and the flare of the original gaseous disc explains also why the flaring depends on metallicity. Taking stars of [Fe/H]= 0.2 and repeating the exercise, we find that the flare is less pronounced than that of [Fe/H]= −0.1 at $t = 0$ (see the right panel of Fig. 7).

The same exercise also explains the origin of vertical metallicity gradients at fixed R. This is shown in Fig. 8, where the red curves indicate the half-mass scaleheight of stars as a function of metallicity, at the present time, and for two different radii, $R = 4$ kpc (left) and $R = 8$ kpc (right). The negative gradients (scaleheights decrease with increasing [Fe/H]) result from the fact that the parent gaseous disc was gradually thinning down as it enriched.

This is confirmed by the blue curves in the same panels, which indicate the half-mass scaleheight of the gas disc *at the time* when its average metallicity at that radius reached the value listed in the abscissa of Fig. 8. In other words, [Fe/H] is a proxy of time for the gas, and, in the absence of substantial accretion, tracks the enrichment process of the gaseous disc. The excellent agreement between the vertical gas evolution and the stellar gradients at $t = 0$ indicate, again, that stars provide, to first order, a snapshot of the properties of the gas disc at the time of their formation.

3.4 Stellar migration after formation

The previous discussion suggests that the kinematics of stars evolve little after their formation. We demonstrate this more explicitly in Fig. 9, where we show the radial profiles of the vertical scaleheight (top) and of the metallicity (bottom) of stars formed at two different lookback times. Dashed lines indicate the properties of such stars at $t = 0$ and solid lines the same at the time of their formation. This figure shows explicitly that there is little radial mixing of stars after their formation: the radial metallicity gradients of stars of given age are essentially the same at $t = 0$ as at the time of formation (bottom panel). There is also little 'heating' in the vertical kinematics of stars after formation: the vertical gradients are again very similar at the time of formation as at $t = 0$ (top panel).

3.5 Vertical thinning of the gas disc

The results presented above indicate that stars of fixed age faithfully trace the properties of the gaseous disc at the time of their formation: their vertical and radial gradients are set at birth, and evolve little thereafter. This elicits two important questions: (i) what determines the vertical scaleheight of the gas, its outward flare, and the timescale of its thinning?; and (ii) since, unlike the gas, stars are not subject to hydrodynamical forces, why do stars trace the properties of the gas so closely?

The scaleheight of an equilibrium gaseous disc is given by the balance between pressure forces and the combined

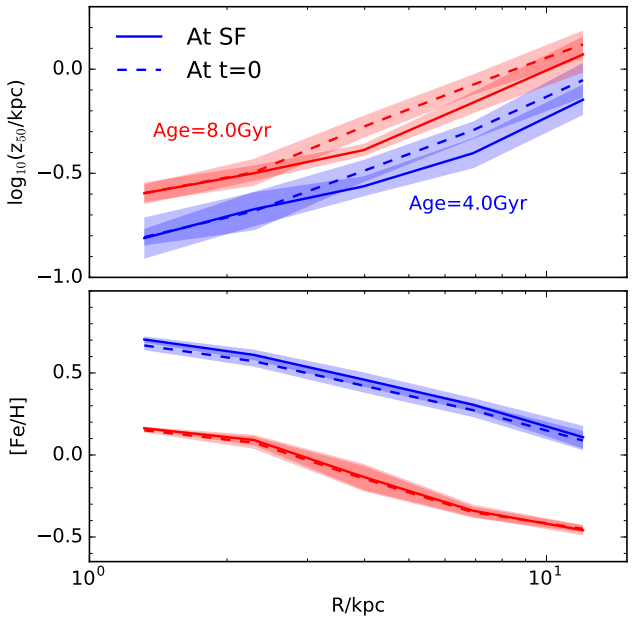

Figure 9. Radial profiles of the vertical half-mass scaleheight (z_{50}; top panel) and metallicity (bottom) of stars shown at the time of their formation (solid line) and at the present (i.e., look-back time $t = 0$; dashed line). Red and blue correspond to stars with age (at $t = 0$) of 4 and 8 Gyr respectively. The weak changes with time indicate that the present-day properties of stars were imprinted largely at birth, and evolved little since their formation.

vertical compressive forces of the dark matter halo and the disc (see Benitez-Llambay et al. 2017, for a recent discussion). For an isothermal gas disc with sound speed c_s, embedded in a dark matter halo with circular velocity profile $V_c(r)$, and surface density profile $\Sigma(R)$, it is straightforward to show that, in the thin disc approximation, the vertical compressive force is given by

$$\frac{\partial \Phi}{\partial z} = \frac{V_c^2}{R}\frac{z}{R} + 2\pi G\Sigma, \qquad (1)$$

where the first term of the right side indicates the contribution of the dark matter halo and the second that of the disc (which may include a stellar component).

When the halo term dominates, the disc is usually termed "non-self-gravitating" (NSG) and its characteristic scaleheight is given by

$$z_{\rm NSG} = \frac{c_s}{V_c(R)}R. \qquad (2)$$

On the other hand, when the disc term dominates the vertical force the disc is "self-gravitating" (SG) and its characteristic scaleheight is given by

$$z_{\rm SG} = \frac{c_s^2}{G\Sigma(R)}. \qquad (3)$$

Because the vertical density law differs when the disc is SG or NSG the characteristic scaleheight values given by Eqs. 2 and 3 are not direct measures of the half-mass scaleheights, z_{50}, which is what we actually shall measure in the simulations. The proportionality factors, however, may be easily computed in each case and may be consulted in Benitez-Llambay et al. (2017).

Note that, in general, we expect isothermal exponential gas discs with flat circular velocity curves to 'flare' outwards, since, in that case, the thickness would be $\propto R$ if non-self-gravitating, and $\propto \Sigma^{-1}$ if self-gravitating.

We compare in Fig. 10 the above expectation with the gas disc half-mass scaleheights measured at two different lookback times, ≈ 10 and ≈ 4 Gyr ago. The thick grey curve shows the result of the simulation, whereas the SG and NSG scaleheights are shown with dotted and dashed red curves, respectively. We use the midplane sound speed to account for the density-dependent EAGLE equation of state; as a result, the effective sound speed in Eq. 2 depends (weakly) on R. The solid red line is the actual expected value when considering the disc and halo combined vertical forces. Clearly the simulated disc is *much thicker* than expected given these considerations, at essentially all radii.

Indeed, what sets the thickness of the disc is actually the balance between the vertical forces and the 'pressure' provided by random bulk motions in the gas. The blue dashed curves in Fig. 10 show again the NSG solution, but replacing the sound speed, c_s, with the vertical velocity dispersion of the gas particles, σ_z, in Eq. 2. The agreement between this curve and the simulation results indicates that the gas disc is kept thick by the vertical random motions of the gas, and, in particular, of the star forming gas clouds that may be clearly seen in the bottom panels of Fig. 4, especially at early times.

These random motions should be quelled on a couple of dynamical timescales, but, as seen in the right panel of Fig. 10, they still dominate in the outskirts of the disc after 6 Gyr of evolution, or more than ≈ 20 circular orbit periods at $R = 10$ kpc. (Orbital times as a function of radius, as well as circular velocity profiles of the simulated galaxy are provided in the Appendix.) The gas disc is actually kept thick by the feedback energy provided by evolving stars—this is deposited as thermal energy in the disc, where it is able to blow bubbles and to push gas outside the disc quite efficiently, especially when star formation rates are high.

We show this in Fig. 11, where we plot the half-mass scaleheight evolution of a gas disc formed in an idealized simulation which evolved a system tailored to match approximately the mass, size, and angular momentum of the gaseous disc at $t = 10$ Gyr (see Fig. 6). In this simulation, gas is allowed to cool and collapse from a ≈ 2 kpc-thick rotating 'slab' embedded in a spherical Navarro-Frenk-White (NFW, Navarro et al. 1996, 1997) dark matter halo potential with parameters chosen to match the circular velocity profile of the galaxy at that time (Fig. 15).

The solid lines in Fig. 11 indicate the evolution of the half-mass scaleheight at two different radii ($R = 4$ and 8 kpc), when the system is evolved in the absence of star formation or feedback. As expected, the disc quickly collapses vertically to a pressure-supported disc roughly ≈ 200 pc thick. The simulation is ended after just ≈ 700 Myr because the disc breaks into massive self-bound clumps, making estimates of its thickness unreliable. When star formation is included, however, the gaseous disc settles into a much thicker structure which is supported by the gas bulk motions induced by the feedback energy released by evolving stars. (See dashed lines in Fig. 11.)

Interestingly, the idealized disc with feedback is still thinner than in the real APOSTLE galaxy (compare with

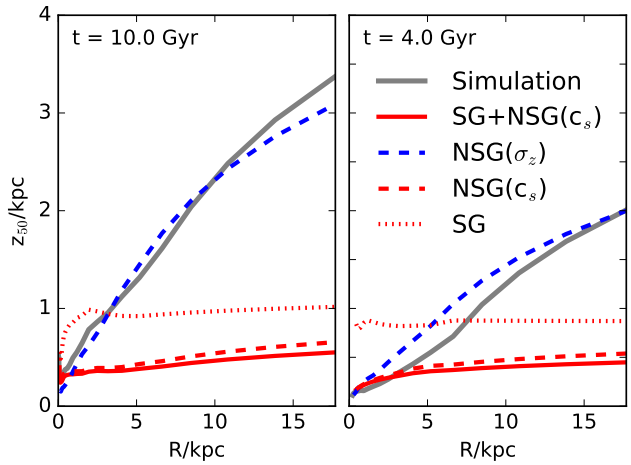

Figure 10. The (strongly flared) vertical half-mass scaleheight profile of the gas at $t = 10$ Gyr and $t = 4$ Gyr (thick grey solid line). Expected scaleheights assuming vertical hydrostatic equilibrium with thermal pressure are indicated for the case of a self-gravitating disc (SG, red dotted) and non-self-gravitating disc (NSG, red dashed). These are generally much smaller than the actual thickness of the simulated disc, which is well matched by the NSG solution but where the 'pressure' support is given by the vertical velocity dispersion of the gas particles (σ_z) rather than by the midplane thermal sound speed (c_s). The disc is largely kept thick by the feedback-induced bulk motions of the gas. (See text for a full discussion.)

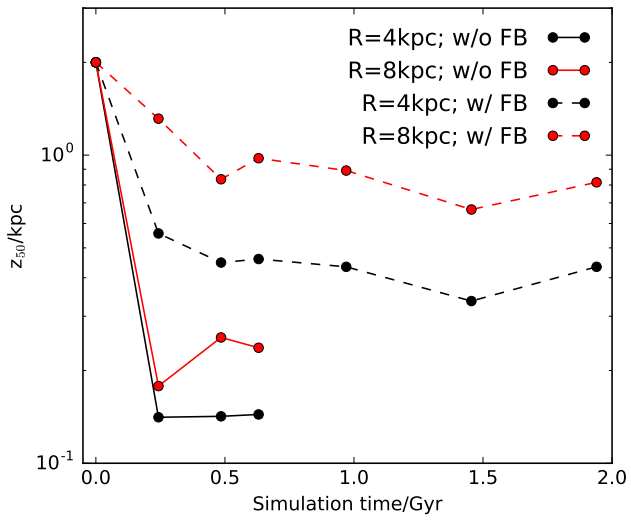

Figure 11. Scaleheight evolution, at two different radii, of an idealized gas disc simulation with (dashed lines) and without (solid lines) the effects of star formation and feedback. Note that the disc is much thicker when including star formation, demonstrating the key role of feedback in stirring up the vertical motions that keep the gas disc thick. See text for details on the idealized simulation.

the left panel of Fig. 10), suggesting that there may be an additional source of vertical support in the APOSTLE simulation, possibly related to bulk motions induced by the continuous gas accretion, which is not included in the idealized runs. In any case, Fig. 11 shows clearly that the thickness of our simulated disc is largely set and controlled by feedback-induced vertical motions in the gas, whose effective pressure far exceeds the thermal support.

Feedback is thus a critical ingredient for understanding the origin of vertical gradients in our simulations, connecting the star formation history at each radius and its consequent enrichment with the evolving thickness of the star forming disc. In this scenario, the disc thins down as the gaseous disc is depleted, star formation abates, and feedback (and, possibly, accretion) heating becomes less effective. A strong prediction is then that the star formation, enrichment, and thinning timescales should all be linked at all radii, as it may have already been observed in the inner Galaxy (see; e.g., Freudenburg et al. 2016).

The same scenario explains why the vertical structure of stars tracks so closely that of the gas at the time of their formation. This is because the star forming gas is best described as a collection of dense clouds with appreciable bulk velocities, rather than as a fluid in vertical hydrostatic equilibrium supported by thermal pressure. Indeed, had stars been born of gas in thermal hydrostatic equilibrium the stellar disc would be much thinner than its parent gas disc due to the loss of vertical pressure (see Benitez-Llambay et al. 2017). In our simulations, however, stars inherit the bulk motions of the gas clouds from which they are born. Since these motions are dominant over thermal pressure forces there is little difference between gas clouds and newly formed stars, explaining why stars trace faithfully the properties of the gas at the time of their formation.

4 A MODEL FOR THE ORIGIN OF METALLICITY GRADIENTS

The scenario discussed above, where gradients result from the intertwined evolution of the gaseous disc's star formation, enrichment, and vertical structure, may be encapsulated in a simple model that can be used to interpret the origin of various chemical and kinematical trends in the Galaxy. The model assumes that stars inherit the properties of the gas at the time of formation and preserve them to the present. It also requires, at a minimum, a characterization of the disc surface density profile, $\Sigma(R)$, its thickness profile, $z_{50}(R)$, and its average metallicity profile, $\langle[\mathrm{Fe/H}]\rangle(R)$, as a function of time.

4.1 Gas disc evolution parametrisation

The evolution of the vertical structure of the gaseous disc may be approximated simply by

$$z_{50}(R) = z_{50,0}\; e^{R/R_z}\; e^{(t/\tau_z)^2}, \qquad (4)$$

where t is lookback time, $z_{50,0} = z_{50}(R = 0, t = 0)$ is the central half-mass disc scaleheight at the present time, R_z is a characteristic flaring radius, and we have assumed that the thinning timescale of the disc, τ_z, is independent of R.

A similar description may be adopted for the evolution of the metallicity gradient. We assume that the average metallicity profile is given by $Z(R,t) = \langle[\mathrm{Fe/H}]\rangle(R,t)$, and that it may be approximated by

$$Z(R,t) = Z_0\,[1+\alpha_0(R/Z_0)]\;\; e^{-(t/\tau_Z)^2}, \qquad (5)$$

where $Z_0 = Z(R=0,t=0)$ is the central average gas metallicity at the present time, $\alpha_0 = (dZ/dR)_{R=0}$, and we have assumed that the enrichment timescale, τ_Z, is independent of R.

We compare these parametrisations with the evolution of the simulated disc in Fig. 12, for three different radii. The thinning and enrichment timescales that best approximate the simulated disc are $\tau_z = 14$ Gyr and $\tau_Z = 9$ Gyr, respectively. This figure shows that the functional forms adopted above are adequate, at least for $t > 4$ Gyr. At more recent lookback times the disc accretes a substantial amount of metal-poor gas (see middle panel of Fig. 2), lowering the average metallicities at all radii. This non-monotonic behaviour cannot be reproduced by our simple formulation.

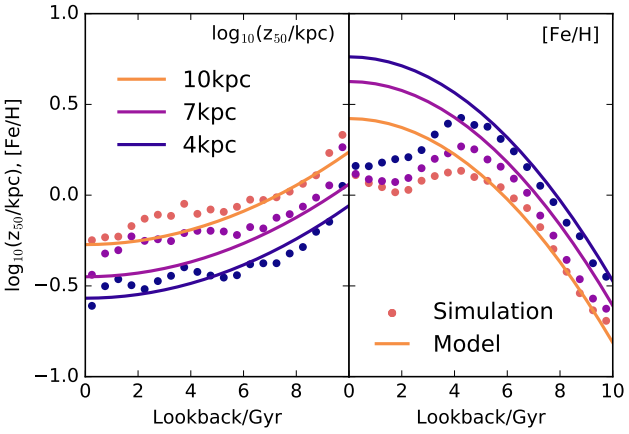

Figure 12. Evolution with lookback time of the gas scaleheight (left) and average metallicity (right) at three different radii: $R = 10$, 7, and 4 kpc. The solid circles indicate the result of the simulation, the thick lines are fits using the parametrisation given in Eq. 4 and Eq. 5.

4.2 Application to the Milky Way

Given the assumptions of the parametrisation adopted above, the radial and vertical gradients that result will be largely set by the flaring profile and metallicity gradient adopted for the gaseous disc at $t = 0$, as well as by the ratio between the thinning timescale, τ_z, and the enrichment timescale, τ_Z. Some intuition may be gained from considering hypothetical cases when one timescale is much longer than the other.

For example, if enrichment proceeded much faster than thinning, then all populations, regardless of metallicity, would have the same flaring profile (that of the gaseous disc), and there would be no vertical metallicity gradient at fixed R. If, on the other hand, thinning proceeded much faster than enrichment, then we would expect strong vertical gradients to develop at fixed R. In this case, the flaring profile of stars of fixed metallicity would depend in detail on the gas disc flare, as well as on the ratio of thinning and enrichment timescales. Depending on these parameters, stars of given Z might show no flare even though the gaseous disc is always flared.

We illustrate this with a simple application to the Milky Way. We emphasize that this is *not* a model of the chemical evolution of the Milky Way disc(s) but rather an illustration of how the results discussed in the previous subsections may be used to interpret the data.

The model requires the present-day gas MW density/metallicity profiles. We show these in the left panels of Fig. 13: the top two show the vertical gas scaleheight profile taken from the fits to 21-cm data presented by Kalberla & Dedes (2008). The gas disc is clearly flared, and can be well approximated, at $t = 0$, by Eq. 4 ($z_{50,0} = 0.06$ kpc and $R_z = 9.8$ kpc), as shown by the bue lines. The bottom-left panel shows the Cepheid metallicity profile from Genovali et al. (2014), which we shall take to represent the present-day radial metallicity profile of the Galaxy midplane, and which we approximate with $Z_0 = 0.5$ and $\alpha_0 = -0.06$ dex/kpc. This gradient can also be approximated by the parametrisation adopted in Eq. 5, as shown by the blue lines in that panel.

The only remaining parameters are τ_z and τ_Z. We choose two cases, again mainly for illustration. Model 1 (M1) assumes $\tau_z \approx \tau_Z$; i.e., $\tau_z = 9.5$ Gyr, and $\tau_Z = 9.0$ Gyr. Model 2 (M2), on the other hand, assumes that thinning proceeds on a much longer timescale than enrichment; i.e., $\tau_z = 19$ Gyr, and $\tau_Z = 9.0$ Gyr. Note that the two models differ only in the thinning timescale.

The evolution of both thickness and average metallicity is shown for three different radii; $R = 10$, 7, and 4 kpc, in the right panels of Fig. 13. In M1 the disc thins down quickly from a much thicker earlier configuration to its final state, whereas it evolves much more gradually in M2. The metallicity evolution is identical in both models, and shows that the disc has enriched at all radii by more than one dex in the past ≈ 10 Gyr.

The effect of these two different evolutionary patterns on the flaring profile of stars of fixed metallicity is shown in the left panels of Fig. 14. In the case of Model 1 the enrichment and thinning timescales are comparable and, for the flaring profile of Kalberla & Dedes (2008), leads to populations of stars that show *no flare* at fixed metallicity.

Model 2, on the other hand, leads to well-defined flares in populations of fixed metallicity, as shown in the bottom-left panel of Fig. 14. Interestingly, both trends are seen in the Milky Way disc, where there is compelling evidence for the presence of two chemically-distinct populations (Bovy et al. 2016): an α-rich disc (the traditional 'thick disc') with no flares (like M1), and an α-poor ('thin') disc whose subpopulations clearly flare outwards (like M2). (See right panels of Fig. 14.)

Although the presence of these flares has been taken as evidence for the effects of radial migration, our results argue that such flares might also result from the gradual thinning of the gaseous disc. This should not be viewed as implying that radial migration does not occur; only that the mere presence of a flare does not guarantee that it has been caused by radial migration, and that other explanations must also be considered.

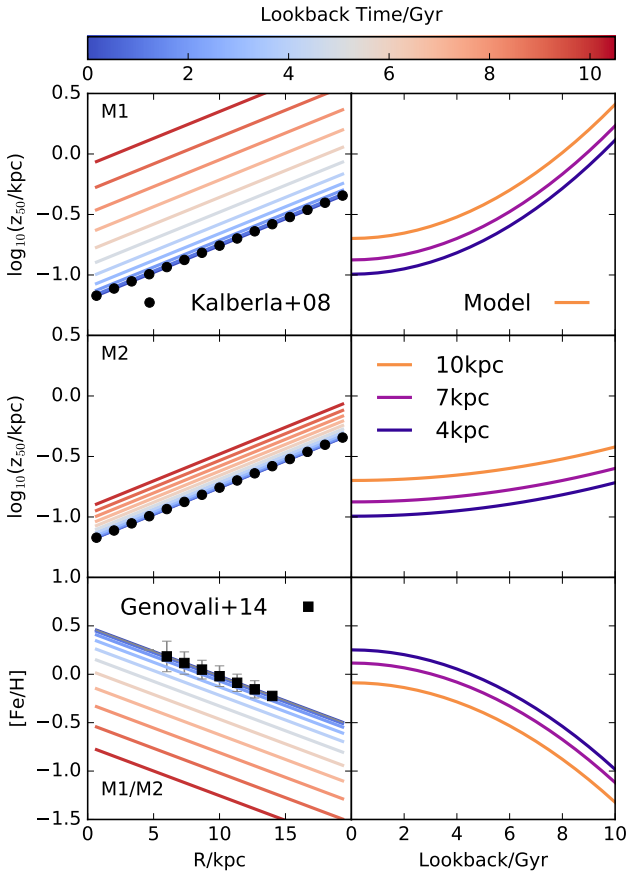

Figure 13. *Left column:* Top and middle panels illustrate the evolution of the gas half-mass scaleheight profile, $z_{50}(R)$, assumed in model 1 (M1) and model 2 (M2), respectively. Bottom panel is analogous, but for the average metallicity profile. The shapes of the final profiles have been chosen to match the exponential fit of Kalberla & Dedes (2008) (top left) and the Cepheid metallicity gradient of Genovali et al. (2014). *Right column:* Scaleheight evolution at three different radii; $R = 10$, 7 and 4 kpc, for M1 (top) and M2 (middle). Bottom panel shows the evolution of the average metallicity at the same radii, which is the same for both models.

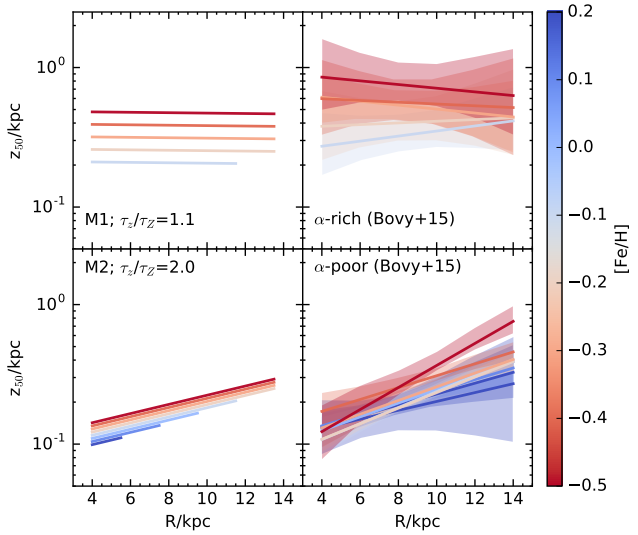

Figure 14. *Left column:* Scaleheight profiles of stars of fixed-metallicity formed out of gas discs evolving as in model 1(top) or model 2 (bottom). Stars are assumed to inherit and preserve the properties of the gaseous disc at birth. *Right column:* A summary of the scaleheight profiles for stars of fixed metallicity, taken from Bovy et al. (2016). Top panel shows that fixed-metallicity stars in the α-rich ('thick') disc show no obvious flares. Stars of the α-poor ('thin') component, on the other hand, flare outward. Either of these trends can be reproduced by models M1 and M2, by adjusting a single parameter, the ratio of enrichment-to-thinning timescale, τ_Z/τ_z. See text for a detailed discussion.

5 SUMMARY AND DISCUSSION

We use a cosmological simulation from the APOSTLE project to study the origin of radial and vertical gradients in the age and metallicity of disc stars. We focus our analysis on one particular galaxy selected because of its overall resemblance to the Milky Way: most stars at lookback time $t = 0$ are in a well defined, coplanar, centrifugally-supported disc component; it has formed stars throughout its history; it has had no recent major mergers; has no major morphological peculiarities; has had a quiet recent merger history; and has formed most of its stars in-situ.

In addition, several of the gradients in the simulated galaxy resemble those of the Milky Way. In particular, average stellar ages and metallicities decrease with increasing radius in the disc midplane; at fixed R, metallicity decreases and age increases with increasing $|z|$; and the disc exhibits a pronounced 'flare' (i.e., the scaleheight of stars of fixed age or metallicity increases monotonically outwards).

We trace the origin of these gradients to the properties of the parent gaseous disc, which first assembles into a thick, slowly-rotating, flared structure and then gradually thins down, settles, and cools kinematically as gas turns into stars and enriches itself in the process. The disc is denser near the centre, and therefore the enrichment and thinning process proceeds more rapidly there than in the outskirts.

Stars inherit the properties of the gas disc at the time of their formation, and evolve little thereafter. In other words, the resulting gradients are predominantly imprinted at birth, and are not the result of secular evolutionary processes such as radial migration or disc instabilities.

The similarity in the vertical structure of stars at late times and that of the gas at the time of their formation results because the gaseous disc is not in thermal hydrostatic equilibrium. Rather, its vertical structure is largely set by the bulk motions of star forming gas clouds, which are in turn induced and sustained by the feedback energy of evolving stars and, possibly, energy injected by continuous gas accretion. As a result, the timescales of star formation, enrichment, and equilibration are all intertwined, and leave behind clear radial and vertical gradients in the gaseous disc and its descendent stars.

Our results suggest that many well-established gradients that are often ascribed to secular evolutionary processes, such as the age-velocity dispersion relation, the vertical age/metallicity gradients, or the outward flare of disc stars of common age or metallicity, may actually be the result of the gradual equilibration process of a star forming, self-enriching disc.

Our simulation is the latest of a number of cosmological simulations of disc galaxy formation that argue that the conditions 'at birth' play a critical role in our understanding of the origin of Galactic gradients (see; e.g., Brook et al. 2012; Bird et al. 2013; Stinson et al. 2013; Miranda et al. 2016; Ma et al. 2017; Grand et al. 2017, and references therein). Although the simulations differ in their details, the qualitative scenario they recount is common to all: a feedback-thickened, star-forming, flared gaseous disc that gradually turns itself into stars as it equilibrates and settles down, results in a disc galaxy that resembles the Milky Way in a surprising number of ways. These simulations also show that internal evolutionary processes (such as migration and vertical thickening) do matter, but are neither responsible for the main structural properties of the galaxies, nor for the origin of their gradients.

This scenario offers a theoretical template that may be used to interpret observations, such as those that will result from ongoing and upcoming surveys of the Milky Way. Its crucial prediction is that locally the timescales of star formation, enrichment, equilibration, and thinning should all be connected through a simple physical model of feedback and accretion. The relations between these timescales and their observational consequences need to be spelled out in more detail by future work to yield falsifiable predictions that may be used to assess the validity and general applicability of this scenario.

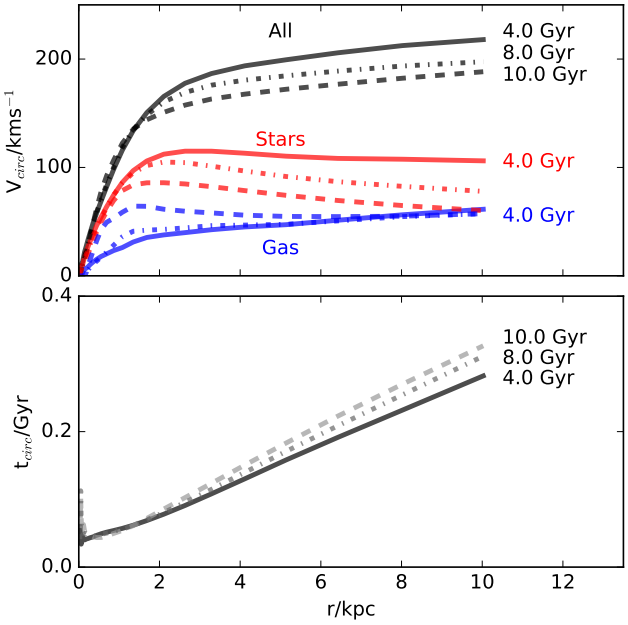

Figure 15. Top panel shows circular velocity profiles (assuming spherical symmetry), $V_{\rm circ}(R) = (GM(R)/R)^{1/2}$, at $t = 0$ and selected lookback times (7.5 and 9.5 Gyr ago). Bottom panel shows the circular orbital time as a function of spherical radius, assuming $t_{\rm circ} = 2\pi r/V_{\rm circ}$, at the same lookback times.

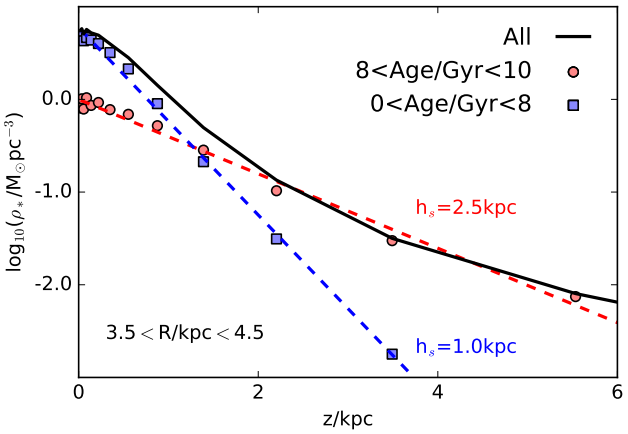

Figure 16. Vertical density distribution, $\rho(z)$, for all disc stars with radii $3.5 < R/{\rm kpc} < 4.5$ (black line). Old stars contribute mostly to a 'thick' disc; young stars to a 'thin' disc, each well approximated by a simple exponential law.

6 ACKNOWLEDGEMENTS

The research was supported in part by the Science and Technology Facilities Council Consolidated Grant (ST/F001166/1), and the European Research Council under the European Union's Seventh Framework Programme (FP7/2007-2013)/ERC Grant agreement 278594-GasAroundGalaxies. CSF acknowledges ERC Advanced Grant 267291 COSMIWAY. This work used the DiRAC Data Centric system at Durham University, operated by the Institute for Computational Cosmology on behalf of the STFC DiRAC HPC Facility (www.dirac.ac.uk). The DiRAC system was funded by BIS National E-infrastructure capital grant ST/K00042X/1, STFC capital grants ST/H008519/1 and ST/K00087X/1, STFC DiRAC Operations grant ST/K003267/1 and Durham University. DiRAC is part of the National E-Infrastructure. This research has made use of NASA's Astrophysics Data System.

7 APPENDIX

We present in this brief appendix, for the sake of completeness and reference, the circular velocity profile of the galaxy at various times (Fig. 15), as well as the vertical density profile of stars at a cylindrical radius $R = 4$ kpc (Fig. 16). The former shows that our galaxy has a reasonably flat circular velocity profile, as commonly observed for spiral galaxies. The latter shows that, as for the Milky Way (Gilmore & Reid 1983), the vertical density profile of stars is not well approximated by a simple exponential law, but can be described by the superposition of a 'thick' and a 'thin' disc.

REFERENCES

Anders F., et al., 2014, A&A, 564, A115
Benitez-Llambay A., Navarro J. F., Frenk C. S., Ludlow A. D., 2017, preprint, (arXiv:1707.08046)
Bensby T., Feltzing S., Lundström I., Ilyin I., 2005, A&A, 433, 185
Bergemann M., et al., 2014, A&A, 565, A89
Bird J. C., Kazantzidis S., Weinberg D. H., Guedes J., Callegari S., Mayer L., Madau P., 2013, ApJ, 773, 43
Boeche C., et al., 2013, A&A, 559, A59

Bournaud F., Elmegreen B. G., Martig M., 2009, ApJ, 707, L1
Bovy J., Rix H.-W., Schlafly E. F., Nidever D. L., Holtzman J. A., Shetrone M., Beers T. C., 2016, ApJ, 823, 30
Brook C. B., et al., 2012, MNRAS, 426, 690
Casagrande L., et al., 2016, MNRAS, 455, 987
Chiappini C., Matteucci F., Romano D., 2001, ApJ, 554, 1044
Crain R. A., et al., 2015, MNRAS, 450, 1937
Davis M., Efstathiou G., Frenk C. S., White S. D. M., 1985, ApJ, 292, 371
Dolag K., Borgani S., Murante G., Springel V., 2009, MNRAS, 399, 497
Eggen O. J., Lynden-Bell D., Sandage A. R., 1962, ApJ, 136, 748
Fattahi A., et al., 2016, MNRAS, 457, 844
Freeman K., Bland-Hawthorn J., 2002, ARA&A, 40, 487
Freudenburg J. K. C., Weinberg D. H., Hayden M. R., Holtzman J. A., 2016, preprint, (arXiv:1608.06342)
Genovali K., et al., 2014, A&A, 566, A37
Gilmore G., Reid N., 1983, MNRAS, 202, 1025
Grand R. J. J., et al., 2017, MNRAS, 467, 179
Hayden M. R., et al., 2014, AJ, 147, 116
Haywood M., Di Matteo P., Lehnert M. D., Katz D., Gómez A., 2013, A&A, 560, A109
Holmberg J., Nordström B., Andersen J., 2009, A&A, 501, 941
Kalberla P. M. W., Dedes L., 2008, A&A, 487, 951
Komatsu E., et al., 2011, ApJS, 192, 18
Ma X., Hopkins P. F., Wetzel A. R., Kirby E. N., Anglés-Alcázar D., Faucher-Giguère C.-A., Kereš D., Quataert E., 2017, MNRAS, 467, 2430
Martig M., Minchev I., Ness M., Fouesneau M., Rix H.-W., 2016, ApJ, 831, 139
Matteucci F., Francois P., 1989, MNRAS, 239, 885
Mikolaitis Š., et al., 2014, A&A, 572, A33
Minchev I., Chiappini C., Martig M., 2013, A&A, 558, A9
Minchev I., Chiappini C., Martig M., 2014, A&A, 572, A92
Miranda M. S., et al., 2016, A&A, 587, A10
Navarro J. F., Frenk C. S., White S. D. M., 1996, ApJ, 462, 563
Navarro J. F., Frenk C. S., White S. D. M., 1997, ApJ, 490, 493
Navarro J. F., Abadi M. G., Venn K. A., Freeman K. C., Anguiano B., 2011, MNRAS, 412, 1203
Ness M., Hogg D. W., Rix H.-W., Martig M., Pinsonneault M. H., Ho A. Y. Q., 2016, ApJ, 823, 114
Quillen A. C., Garnett D. R., 2001, in Funes J. G., Corsini E. M., eds, Astronomical Society of the Pacific Conference Series Vol. 230, Galaxy Disks and Disk Galaxies. pp 87–88
Recio-Blanco A., et al., 2014, A&A, 567, A5
Rix H.-W., Bovy J., 2013, A&ARv, 21, 61
Sawala T., et al., 2016, MNRAS, 457, 1931
Schaye J., et al., 2015, MNRAS, 446, 521
Springel V., White S. D. M., Tormen G., Kauffmann G., 2001, MNRAS, 328, 726
Stinson G. S., et al., 2013, MNRAS, 436, 625
Venn K. A., Irwin M., Shetrone M. D., Tout C. A., Hill V., Tolstoy E., 2004, AJ, 128, 1177
Wielen R., 1977, A&A, 60, 263